Journal of Materials Chemistry A

Accepted Manuscript

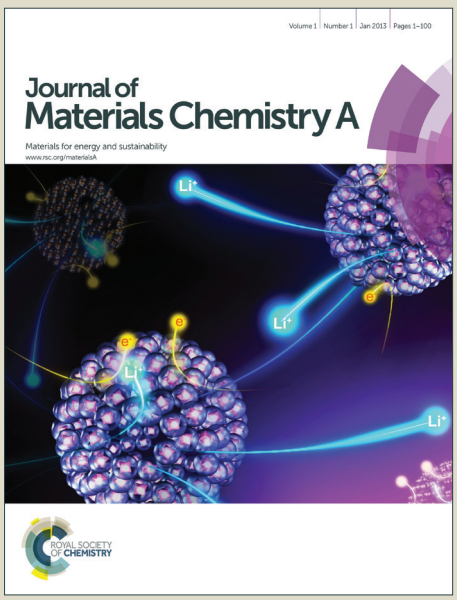

This is an *Accepted Manuscript*, which has been through the Royal Society of Chemistry peer review process and has been accepted for publication.

Accepted Manuscripts are published online shortly after acceptance, before technical editing, formatting and proof reading. Using this free service, authors can make their results available to the community, in citable form, before we publish the edited article. We will replace this *Accepted Manuscript* with the edited and formatted *Advance Article* as soon as it is available.

You can find more information about *Accepted Manuscripts* in the Information for Authors.

Please note that technical editing may introduce minor changes to the text and/or graphics, which may alter content. The journal's standard Terms & Conditions and the Ethical guidelines still apply. In no event shall the Royal Society of Chemistry be held responsible for any errors or omissions in this *Accepted Manuscript* or any consequences arising from the use of any information it contains.

ROYAL SOCIETY OF CHEMISTRY

www.rsc.org/materialsA

Journal of Materials Chemistry A

Dynamic Article Links ►

Cite this: DOI: 10.1039/c0xx00000x

PAPER

www.rsc.org/xxxxxx

A Two Dimensional Highly Ordered Mesoporous Carbon/Graphene Nanocomposite for Electrochemical Double Layer Capacitors: Effect of Electrical and Ionic Conduction Pathways

Chang-Wook Lee,[a] Seung-Beom Yoon,[a] Hyun-Kyung Kim,[a] Hee-Chang Youn,[a] Joah Han,[b] Kwang Chul Roh,*[b] and Kwang-Bum Kim*[a]

Received (in XXX, XXX) Xth XXXXXXXXX 20XX, Accepted Xth XXXXXXXXX 20XX
DOI: 10.1039/b000000x

A two dimensional highly ordered mesoporous carbon/graphene nanocomposite (MCG) was synthesized by replicating a KIT-6/graphene nanocomposite. The MCG exhibited a high Brunauer–Emmett–Teller surface area of 1179 m^2 g^{-1} and a large total pore volume of 0.94 cm^3 g^{-1}. On account of its large surface area and high electrical conductivity with 2D morphology, MCG showed a very high specific capacitance of 276 F g^{-1} at 1 A g^{-1} and maintained 86% of initial capacitance at 100 A g^{-1} in 1.0 M TEABF4/AN.

Introduction

Electrochemical capacitors (ECs), also called supercapacitors, are energy storage devices with a promising combination of features such as high power density and excellent cycling stability,[1-3] However, supercapacitors are not yet capable of delivering high energy densities comparable to those of secondary batteries, and this drawback restricts the use of supercapacitors mainly to high-power applications such as emergency power supplies, electronic vehicles and portable power tools.[4] According to the energy storage mechanism, supercapacitors can be categorized as either electrochemical double layer capacitors (EDLCs) or pseudocapacitors.[3] EDLCs are based on double layer capacitance, caused by charge separation at the electrode/solution interface, while pseudocapacitors are based on the pseudocapacitance resulting from faradaic redox reactions occurring at the surface layer of electroactive materials. Considering the charge storage mechanism of EDLC, the specific surface area of electrode material is a critical factor to the capacitance of EDLC. For that, activated carbons are usually prepared by a chemical activation method (using an activating agent such as KOH or NaOH) in order to attain high surface area.[5, 6] However, activated carbons suffer from poor electrical conductivity and random micropore structures caused by severe chemical activation. It has been reported that relatively low specific capacitance and poor capacitance performance at high rates of activated carbons are due to the presence of micropores that are inaccessible by the electrolyte, wetting deficiencies of electrolytes on electrode surface, and/or the inability of a double layer to form successfully in the pores.[7, 8] In addition to specific surface area, therefore, effective pore size, continuously interconnected pore structure, good electrical conductivity and ionic conductivity should be considered in the design and synthesis of EDLC electrode materials.[9-12]

Recently, porous carbon materials such as ordered mesoporous carbon, carbon aerogel, carbide-derived carbon (CDC) and graphene have recently been reported as potential alternatives of activated carbons.[12-17] Among those porous carbon materials, mesoporous carbons have been investigated as candidate materials due to their high surface area, suitable pore size and continuously interconnected pore structure.[17-22] Regularly interconnected pore structure in the mesopore size range in particular is expected to be favorable for ionic transport.[23-25] Xing et al. have reported the ordered mesoporous carbons with a specific capacitance of 206 F g^{-1} at 5 mV s^{-1} in 6.0 M KOH electrolyte. According to their analysis, the ordered mesoporous carbons could maintain 80% of initial capacitance at 50 mV s^{-1}, while commercial activated carbon Maxsorb could have only 20%.[25] It indicates the importance of the ordered pore structure of carbon to the material's rate capability. However, further improvement in rate capability of ordered mesoporous carbons is still hindered by their particulate morphology and larger particle size and high electric resistance originated from the porous nature.[20] Even with ordered mesoporous carbons, ion transport is strongly affected by diffusion length of the electrolyte ions as well as ordered pore structure.[26-28] A recent study about the effect of particle size of CDC from the view of the diffusion length of the electrolyte ions reported that the time constant decreased from 5 to 3.5 s, when decreasing the particle size from 20 um to 20 nm.[29]

Ordered mesoporous carbons are usually prepared through templating approaches using mesoporous silicas.[30-32] Sucrose, combined with sulfuric acid as a catalyst, is the most commonly used precursor for mesoporous carbon preparation and is heat-treated at temperatures around 900°C. However, the resulting

Journal of Materials Chemistry A Accepted Manuscript

carbons show little to no graphitic character when processed at 900°C, and thus relatively poor electrical conductivity.[33] Heat treatment of ordered mesoporous carbons at higher temperatures around 2300°C could improve the electrical conductivity of mesoporous carbon though graphitization, however, structural deformation is inevitable in most cases. [33-38] [33-38] [33-3834-39] Therefore, new strategy is needed to improve the electrical conductivity of ordered mesoporous carbons while preserving their inherent ordered mesoscopic structural properties. Combining ordered mesoporous carbon and highly conductive material would result in a combination of efficient transport of electrolyte ions through the ordered mesopore structure and high electrical conductivity from highly conductive material.

Two-dimensional (2D) nanomaterials, characterized by nanoscale thickness and infinite length, show promising potential for application in sensors and energy storage and conversion devices.[39-41] In particular, graphene, composed of a single layer of carbon atoms tightly packed into a 2D honeycomb-like sp^2-hybridized carbon lattice, has attracted tremendous attention owing to its unique properties such as its ultrahigh electron mobility, large surface area, ballistic charge carrier transport.[42, 43] These studies have triggered wide interest in graphene based 2D nanosheets for energy storage materials such as carbon/graphene, transition metal oxide/graphene and conducting polymers/graphene nanocomposites.[44-48] Since ordered mesoporous carbon with plentiful mesoporous tunnels is beneficial to the rapid diffusion of the electrolyte, the 2D ordered mesoporous carbon/graphene composites would not only inherit the excellent electrical conductivity of graphene, but also have the advantages of good electrolyte-accessibility and short diffusion length from the 2D ordered mesoporosity. There are a few studies reported about 2D mesoporous carbon/graphene nanocomposites. Yang *et al*. reported the disordered mesoporous carbon/graphene sandwich structure (surface area: 910 $m^2 g^{-1}$) using a disordered mesoporous silica/graphene composite as a hard template.[39] Their 2D mesoporous carbon/graphene nanocomposite was tested as anode materials of lithium ion batteries. Wang *et al*. very recently reported the synthesis of disordered mesoporous carbon/graphene composite (pore size: 4 nm, surface area: 546 $m^2 g^{-1}$) using triblock copolymer (F127) as a soft mesopore-directing template.[19] The mesoporous carbon/graphene composite showed a high specific capacitance of 242 F g^{-1} at a current density of 0.5 A g^{-1} in 6.0 M KOH electrolyte and maintained 58% of initial capacitance at 10 A g^{-1}. The rate capability is not that impressive, considering the 2D mesoporous carbon and graphene constituents in the composite. Similarly, Li *et al*. reported the disordered mesoporous carbon decorated graphene using F127 as structure directing agent (pore size: 6.3 nm, surface area: 927 $m^2 g^{-1}$).[20] The composite showed a capacitance of 213 F g^{-1} at a current density of 0.5 A g^{-1} in 6.0 M KOH electrolyte and maintained 81% of initial capacitance at 20 A g^{-1}. Also, several studies which show the importance of mesoporous carbon/graphene nanocomposites for neighboring (with respect to EDLC devices) fields such as CDI (capacitive deionization), adsorptions and DSSCs (dye-sensitized solar cells).[49-51] Nevertheless, highly ordered mesoporous carbon/graphene composites have not been reported yet.

In the present study, we have successfully synthesized the 2D highly ordered mesoporous carbon/graphene nanocomposites using a KIT-6/graphene nanocomposite as a hard template. The nanocomposite showed a nanosheet-like 2D morphology with a highly ordered mesoporous structure and improved electrical conductivity. Most importantly, the highly ordered mesoporous carbon/graphene nanocomposite could act as a superior electrode material for EDLCs showing excellent capacitance and outstanding high-rate capability in 1.0 M $TEABF_4$/AN. Furthermore, symmetric two-electrode cell assembled with highly ordered mesoporous carbon/graphene nanocomposite showed a remarkable power and energy density, implying the great potential as an electrode material for EDLCs.

Experimental

Preparation of KIT-6/graphene nanocomposite

KIT-6/graphene nanocomposite was synthesized following the procedure reported by our previous research.[52] Graphite oxide (GO) was prepared by a modified Hummers method from purified natural graphite powder (≤ 45μm, Aldrich).[53] As in a typical synthesis, 6 g of P123 ($EO_{20}PO_{70}EO_{20}$, MW = 5800, Aldrich) was dissolved in 217 g of distilled water, 6 g of butanol (Aldrich, 99.4%), and 11.8 g of concentrated HCl (35%); 1 g of GO was stirred into the solution at 35°C for 24 h, and 12.9 g of TEOS (Tetraethoxysilane, ACROS, 98%) was subsequently added at 35°C. The mixture was again stirred for 24 h at 35°C and subsequently refluxed for 1 h at 100°C under microwave irradiation (STARTSYNTH LabStation, Milestone, USA). The microwaved KIT-6/GO was filtered and dried at 100°C, heated at 400°C in air, subsequently heated at 700°C in 5 wt% H_2/Ar to prepare the KIT-6/graphene nanocomposite.

Preparation of two dimensional highly ordered mesoporous carbon/graphene nanocomposite

The 2D highly ordered mesoporous carbon/graphene nanocomposite (denoted as MCG) was prepared by replicating the KIT-6/graphene nanocomposite. KIT-6/graphene nanocomposite was infiltrated with a carbon source of sucrose twice. The first infiltration was performed with a mixture of 1.1 g sucrose, 0.1 g H_2SO_4 and 4.3 g H_2O per gram of KIT-6/graphene nanocomposite. The mixture was heated at 100°C for 1 h and then at 160°C for 1 h. The resultant mixture was repeatedly infiltrated again with sucrose and H_2SO_4. Then, the mixture was carbonized at 900°C under nitrogen. The 2D highly ordered mesoporous carbon/graphene nanocomposite was collected after dissolving the silica template with 1.0 M NaOH solution. For comparison, ordered mesoporous carbon was separately prepared using KIT-6 mesoprous silica particles as a template. (denoted as MC)

Characterization

Transmission electron microscopy (TEM) images were recorded on a Philips CM200 microscope operated at 200 kV. Scanning electron microscopy (SEM) images were recorded on a Hitachi S-4300SE microscope operated at 15 kV. The low-angle X-ray diffraction (XRD) patterns were recorded on a Rigaku D/MAX 2200V/PC X-ray diffractometer with Cu Kα radiation (40 kV, 20 mA) in the range 2θ = 0.8–5° at 0.2° intervals. The Fourier transform infrared (FT-IR) spectra for the samples in KBr pellets

Journal of Materials Chemistry A Accepted Manuscript

This journal is © The Royal Society of Chemistry [year]

were recorded on a Mattson 3000 FT-IR spectrometer in attenuated total reflection (ATR) mode. The spectra were generated in the range 500–4000 cm^{-1} with a 4 cm^{-1} resolution over 120 scans. The Raman spectra were measured using a Jobin-Yvon LabRam HR with a liquid-N_2-cooled charge-coupled device (CCD) multichannel detector at room temperature and conventional backscattering geometry. The nitrogen adsorption-desorption isotherms were measured on a Micromeritics ASAP ZOZO at 77 K, and the surface area was calculated using the Brunauer-Emmett-Teller (BET) method. The XPS measurements were performed using an Omicron ESCA Probe (Omicron Nanotechnology, Taunusstein, Germany) with monochromated Al Kα radiation (hv = 1486.6 eV).

Electrical conductivity of the samples was measured by I-V curve measurement with a pellet in the form of a disc, using 2-point probe method in a cell (VMP2, Biologic). In order to eliminate the contribution of the contact resistance, samples were pressed to different thicknesses. Then, the resistance (R) was plotted against the thickness (t) of the pellet. The electrical conductivity (κ) was calculated according to the following equation:

$$R = \rho\,(t/A) = 1/\kappa\,(t/A) = t/(\kappa A) \quad (1)$$

where R, ρ, κ, t and A are the resistance, resistivity, conductivity, thickness of the pellet and area of the electrode, respectively.

Preparation of electrodes and electrochemical measurement

Electrochemical properties were investigated at room temperature using a CR2032 coin cell. The electrode consisted of a mixture of 90 wt% of active materials (MCG or MC) and 10 wt% polyvinylidene fluoride dissolved in N-methylpyrrolidone as a binder. No additional conductive carbon was used in the electrode preparation. The slurry mixture was coated on aluminum foil (99.7% purity, Aldrich) and then dried at 100 °C for 24 h in air. Each working electrode had an area of 1 cm^2 and contained 1 mg of the dried slurry. The density of the MCG electrode is 0.6 g cm^{-3}. The electrolyte was 1.0 M $TEABF_4$ dissolved in acetonitrile (AN). The coin cells were assembled in an Ar-filled glove box using a microporous polyethylene film (Celgard 2400) as separator. Galvanostatic charge–discharge tests, cyclic voltammetry (CV) and impedance spectroscopy (EIS) were performed on the coin cells using a potentiostat/galvanostat (VMP3, Princeton Applied Research). EIS measurements were carried out in the frequency range of 100 kHz to 100 mHz at 1.35 V with a 5 mV AC amplitude.

The gravimetric specific capacitance per a single electrode (C_{sp}) was calculated from the cyclic voltammograms and galvanostatic charge/discharge data according to the following equations, respectively[54-56] :

$$C_{sp,\,CV} = \int I\Delta V/mvV \quad (2)$$

$$C_{sp,\,Discharge} = I\Delta t/Vm \quad (3)$$

where, I, V, m, v, and Δt represent the applied current, potential window, mass of a single electrode, potential scan rate and discharge time respectively.

The capacitance–frequency dependence from EIS data was obtained according to the following equations[21, 54]:

$$C_{EIS} = -1/2\pi f(Z' - Z'') \quad (4)$$

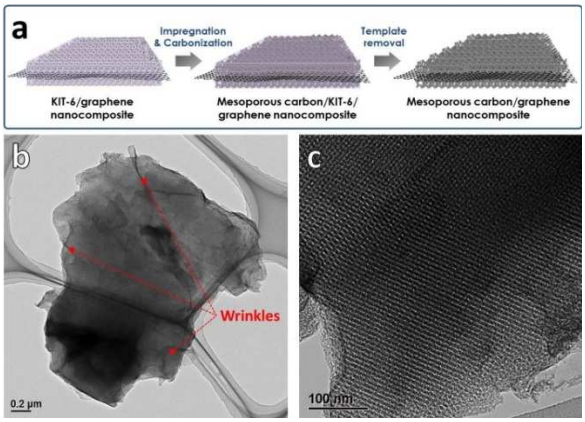

Fig. 1. (a) A schematic illustration of the process adopted for the synthesis of MCG, (b) typical TEM and (c) HRTEM image of MCG.

where, f, Z' and Z'' represent the measurement frequency, real part and imaginary part of the impedance, respectively. The specific capacitance per a single electrode ($C_{sp,\,EIS}$) was calculated from real part in C_{EIS} at the lowest frequency.

Also, the energy density (E) and power density (P) of the unit cell were determined according to the following equations[8, 57] :

$$E = 1/2\ C_{cell}V^2 \quad (5)$$

$$P = E/\Delta t \quad (6)$$

where, C_{cell} $(= 1/4\ C_{sp})$, V, and Δt represent the specific capacitance of the total cell, the potential window, and discharge time, respectively.

Results and discussion

In this study, KIT-6/graphene nanocomposite (denoted as KG) was employed as a hard template. The synthetic procedure and structural properties of KG are well described in our previous research.[52] KG possessed nanosheet-like morphology with a highly ordered Ia3d cubic mesoporous structure (pore size: 4, 6 nm, pore volume: 1.0 $cm^3\ g^{-1}$, surface area: 946 $m^2\ g^{-1}$). With the unique 2D flaky morphology with ordered mesoporous structure, KG could act as a template for the preparation of mesoporous material/graphene nanocomposites. Fig. 1a shows a schematic illustration of the procedure used in the synthesis of the 2D highly ordered mesoporous carbon/graphene nanocomposite (MCG). The first step is the infiltration of sucrose as a carbon precursor into the pores of KG template. The infiltrated sucrose in the KG template is then carbonized at 900°C under N_2 atmosphere. Finally, MCG is obtained after the silica template removal from the composite.

The formation of the 2D highly ordered mesoporous structure on the graphene surface was firstly confirmed using TEM. The TEM images clearly show that the MCG template successfully replicated the KG (see supporting information Fig. S1). Fig. 1a is the low-magnification TEM image of the MCG. The entire image is perfectly transparent under the electron beam. The MCG clearly shows a very thin 2D flaky morphology consisting of folded and wrinkled sheets similar to that of graphene flakes.[58] Furthermore, it is clear that the 2D mesoporous carbons were uniformly coated onto the graphene flake surfaces. And the highly ordered arrays of the pore channels of mesoporous carbons can be clearly seen from Fig. 1b. The mesoporous carbon loading in the nanocomposite was calculated to be 81 wt% from the

Journal of Materials Chemistry A Accepted Manuscript

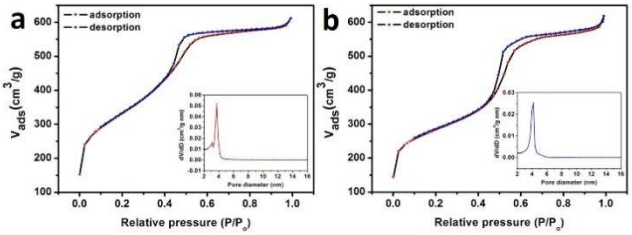

Fig. 2. Typical N_2 adsorption isotherms and pore size distribution of (a) MCG and (b) MC.

molar feeding ratio of sucrose to graphene. Meanwhile, no transparent flaky image is observed in the TEM image of mesoporous carbon (synthesized without graphene, denoted as MC), suggesting that MC has the irregular particulate morphology of MC particles (see supporting information Fig. S2 and Fig. S3). Considering the morphology of the templates (*i.e.*, KG and KIT-6), it is reasonable that the MCG and MC show totally different morphologies.[52]

N_2 adsorption/desorption isotherms and pore-size distributions for the MCG and MC are shown in Fig. 2. Gas adsorption is the most direct method of measuring the specific surface area, pore-size distributions, and pore volume of mesoporous materials. Mesoporous adsorbents with type IV isotherm shows the following important features in the N_2 adsorption/desorption behaviors: (i) a knee point indicating the completion of monolayer coverage and (ii) hysteresis loops associated with capillary condensation in mesopores structures.[59, 60]

MCG in Fig. 2a exhibits a knee for the first adsorption step at a relative vapor pressure of ~0.1 and a hysteresis loop at relative vapor pressures in the range 0.4–0.8. MCG shows a typical type IV isotherm with a type H1 hysteresis loop. MCG had a high Brunauer–Emmett–Teller surface area of 1179 m^2 g^{-1} and a total pore volume of 0.94 cm^3 g^{-1}. Furthermore, MCG exhibit bimodal pores of 3.1 and 3.7 nm, which are characteristic of KIT-6 and graphene flakes, respectively. However, the peak intensity attributable to the mesopores originating from the graphene flake (3.1 nm) was reduced compared to that of the graphene from the KIT-6/graphene nanocomposite, which might be due to the partial change in graphene morphology during the carbonization performed at 900°C.[52] On the other hand, MC in Fig. 2b showed type IV isotherms with a type H1 hysteresis loop and exhibited a BET surface area of 998 m^2 g^{-1}, a pore volume of 0.96 cm^3 g^{-1}, and an average pore size of 4.2 nm, which are consistent with the previously reported literature values.[61, 62]

Low-angle X-ray diffraction (XRD) was used to confirm that the MCG prepared in this study showed a highly ordered mesoporous structure. Fig. 3a shows the low-angle XRD patterns for MCG and KG. KG showed a sharp and intense peak corresponding to the (211) plane and a hump in the (332) plane, clearly demonstrating the formation of a bicontinuous Ia3d mesoporous structure. MCG also shows the low-angle XRD pattern corresponding to Ia3d cubic structure, indicating MCG is an inverse replica of the KG template. It should be noted that the superstructure was slightly contracted, as evidenced by the slight shift of the low-angle XRD peaks of (211) and (332) toward a higher angle. Previously, superstructure contraction has been reports after replication.[62-64] Fig. 3b shows the low-angle XRD pattern for the MC with Ia3d mesoporous structure.

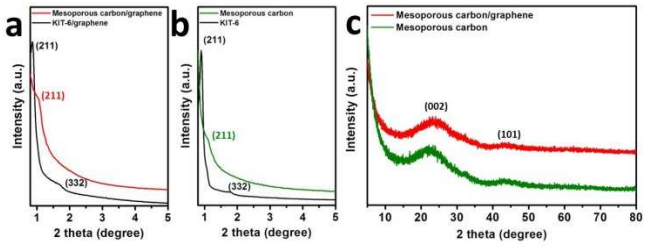

Fig. 3. Low angle XRD patterns of (a) MCG and KG, (b) MC and KIT-6 and (c) wide angle XRD patterns of MCG and MC.

Fig. 3c shows the wide-angle XRD patterns for MCG and MC. The two mesoporous carbons show similar diffraction peaks at ~25 and 43° corresponding to the (002) and (101) diffractions for graphitic carbon.[31, 65] However, the peaks are broad for both MCG and MC, indicating an amorphous carbon framework. The poor graphitic crystallinity of sucrose derived mesoporous carbon under 900°C is previously reported.[33, 34] It can be inferred that MCG and MC consist of a poorly organized carbon with small quantities of graphitized carbon embedded in its structure.

Fig. 4a shows the survey scans indicating that MCG and MC had the same elemental composition. The spectra for MCG and MC show C1*s* and O1*s* peaks at ~284 and ~532 eV, respectively, owing to surface oxygen species. The carbonization degrees of MCG and MC were obtained from the ratio of the C1*s* and O1*s* peak areas. The C/O ratios for MCG and MC were 14.63 and 13.58, respectively. The similar C/O ratios for the MCG and MC are reasonable considering that the infiltrated sucrose was heat-treated under the same conditions. The slightly higher C/O ratio for the MCG is probably due to the presence of graphene in the composite. The high-resolution C1*s* spectra for MCG and MC are shown in supporting information Fig. S4. These spectra are similar, indicating that chemical composition and bonding between carbon and oxygen for MCG and MC are almost identical. Fig. 4b shows the C1*s* XPS spectrum for the MCG. The spectrum was fitted using a Gaussian-Lorentzian peak shape after the Shirley background correction was performed. The binding energy of the C–C and C–H bonds was assigned at 284.5 eV, and chemical shifts of +1.0, +2.5, and +4.0 eV were typically assigned for the C–OH, C=O, and O=C–OH functional groups, respectively.[66-68]

Fig. 5a shows the Raman spectra for MCG and MC. The spectra clearly show strong and weak peaks at ~1580 and 1340 cm^{-1}, respectively. The peak at 1610 cm^{-1} (G band) is attributed to the vibration of sp^2-bonded carbon atoms in a 2D hexagonal lattice; namely, the stretching modes of C=C bonds of typical graphite, while the peak at 1340 cm^{-1} (D band) is associated with

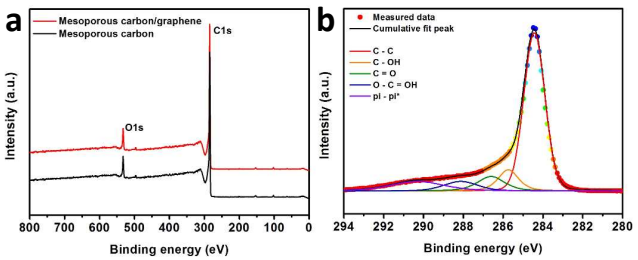

Fig. 4. (a) Full-scale XPS profile for MCG and MC, (b) deconvoluted C1s XPS profiles for MCG

Journal of Materials Chemistry A Accepted Manuscript

This journal is © The Royal Society of Chemistry [year]

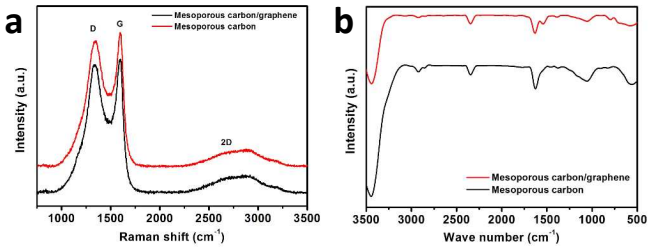

Fig. 5. (a) Raman spectra and (b) FT-IR spectra of MCG and MC

the vibrations of carbon atoms with dangling bonds in the plane terminations of the disordered graphite and is related to the defects and disorders in the structures in carbon materials. In addition, the weak broad 2D peak observed at ~2700 cm^{-1} is caused by second-order zone boundary phonons.[69] The intensity ratios of I_G/I_D for MCG and MC were 1.07 and 1.04, respectively. Considering the loading amount of mesoporous carbon (81 wt.%) in MCG, the slight difference in I_G/I_D ratios between MCG and MC is reasonable. Slightly higher I_G/I_D ratio for the MCG is probably due to the presence of graphene in the nanocomposite.

Fig. 5b shows the FT-IR spectra for MCG and MC. The spectra for both carbons show strong, broad absorption peak at 3400 cm^{-1} due to the O–H stretching vibration and weak absorption peaks at 1228, 1720 and 900, and 1072 cm^{-1} attributed to the hydroxyl, carboxyl, and epoxide functional groups, respectively. The similar spectra for MCG and MC suggest that two mesoporous carbons had similar chemical properties. However, the new absorption band at 1540 cm^{-1} for MCG could be attributed to the skeletal vibration of the graphene sheets.[70-72] Furthermore, the electrical conductivity measurement revealed the positive effect of the graphene on the formation of effective electrical conduction pathways in MCG. As expected, graphene flakes in the nanocomposite resulted in the increased electrical conductivity of the MCG. The electrical conductivity of MCG and MC were found to be 72 and 35 S m^{-1}, respectively.[73, 74]

Cyclic voltammetry, galvanostatic charge/discharge test and EIS measurements were used to investigate the electrochemical properties of MCG and MC. The electrochemical properties were evaluated using the symmetric two-electrode cell system in 1.0 M $TEABF_4$/acetonitrile (AN) electrolyte.

The electrochemical properties of MCG were first analyzed using cyclic voltammetry (CV). Fig. 6a shows the CV curves for the MCG measured in the potential scan rate of 10–1000 mV s^{-1}. MCG shows a typical rectangular shaped cyclic voltammogram at a low scan rate of 10 mV s^{-1}, indicating a typical ideal EDLC behavior. Furthermore, MCG could retain the rectangular shaped voltammograms with little distortion even at the potential scan rate as high as 1000 mV s^{-1}, demonstrating a highly reversible electrochemical behavior with excellent rate capability. It is to be noted that no pseudocapacitive behavior was observed when MCG was tested in 1.0 M $TEABF_4$/acetonitrile (AN) electrolyte. Fig. 6b shows the cyclic voltammograms for MC. At lower scan rates, MC showed rectangular shaped cyclic voltammogram, however, its voltammograms were already severely get distorted even at potential scan rate 200 mV s^{-1}.

Fig. 6c-d show the discharge curves of MCG and MC at current densities ranging from 1 to 100 A g^{-1}. The current densities were normalized with respect to the mass of a single electrode. All the discharge curves in Fig. 6c resemble isosceles triangular shapes, demonstrating an ideal capacitor behavior, even when the current density is as high as 100 A g^{-1}. Each discharge curve clearly shows a linear decline of potential at the given operating voltage, which is characteristic of ideal capacitive behavior. Furthermore, negligible IR drop was observed at the high current density of 100 A g^{-1}, suggesting that the MCG composite electrode is highly conductive even though no

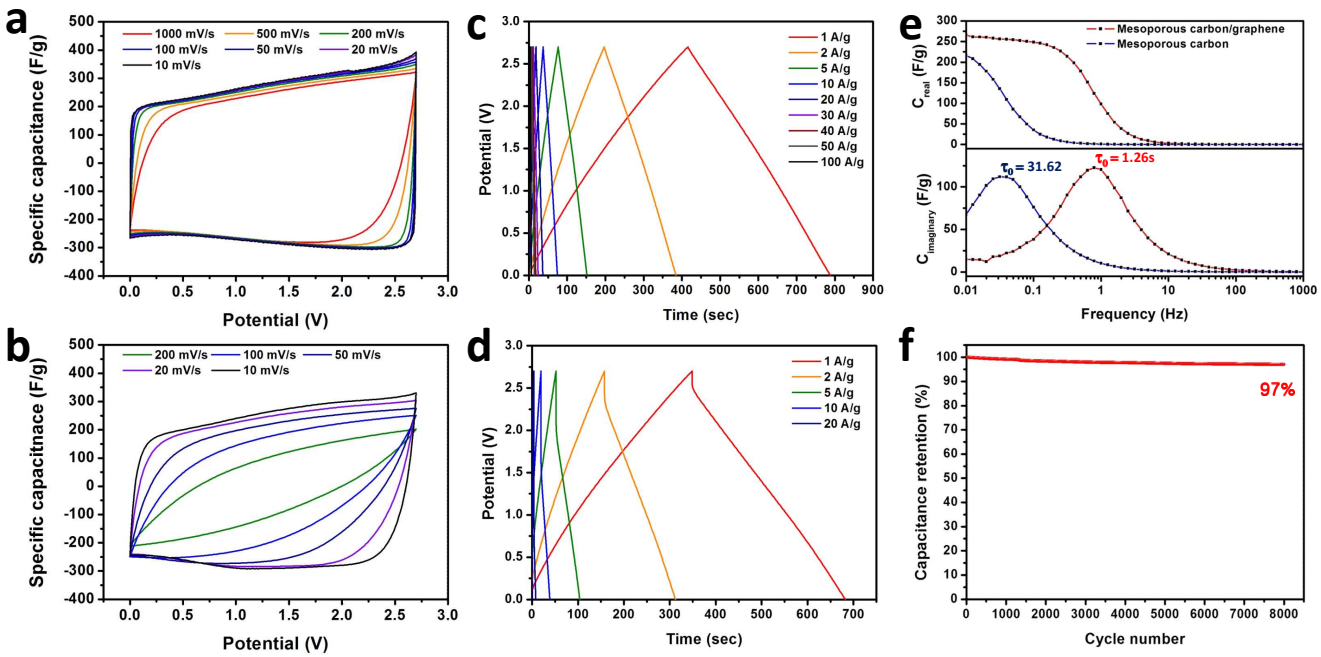

Fig. 6. Cyclic voltammograms of (a) MCG and (b) MC at various scan rates at a scan rates of 10–1000 mV s^{-1} and galvanostatic discharging profiles of (c) MCG and (d) MC at different current densities of 1–100 A g^{-1}, (e) capacitance–frequency dependence from impedance spectroscopy measurements of MCG and MC and (f) cyclability of MCG at 30 A g^{-1}.

Journal of Materials Chemistry A Accepted Manuscript

additional conductive agent was used in the electrode preparation. The MCG showed a high specific capacitance of 276 F g^{-1} at 1 A g^{-1}. The specific capacitance was normalized with respect to the mass of a single electrode. In Fig. 6a, it takes 540 s per one CV cycle at a scan rate of 10 mV s^{-1} and the specific capacitance is calculated to be 255 F g^{-1}. Considering the rate of 788 and 385 s per cycle in the galvanostatic experiments and the specific capacitance of 276 and 275 F g^{-1} at 1 and 2 A g^{-1}, respectively, the specific capacitance from both kinds of experiments shows similar performance at comparable rates. More importantly, capacitance retention, which is the ratio of specific capacitance at 20 A g^{-1} to that at 1 A g^{-1}, as 97%, demonstrating an excellent rate capability. Furthermore, it maintains 86% of initial capacitance even at 100 A g^{-1}. It is consistent with little distortion of the cyclic voltammograms observed with an increase in the potential scan rate. Generally, mesoporous carbons show higher specific capacitances while graphene materials show better rate capabilities.[13, 75-82] Compared with previous researches, the specific capacitance and high rate capability are comparable with mesoporous carbon and graphene based nano-materials, respectively (see supporting information Fig. S5). The MC showed a specific capacitance of 247 F g^{-1} at 1 A g^{-1}, which is comparable to that of MCG. However, MC shows much larger IR drops compared with MCG at same discharge current density. Therefore, MC could have a specific capacitance of 61 F g^{-1} at 20 A^{-1}, indicating a very low capacitance retention of 25%. It might be due to a large decrease in the utilization of the effective surface area of MC as the discharging current is increased. In MCG, graphene acts as a 2D conductive template to provide a 2D conduction path in the composite and a template for the 2D ordered mesoporous carbon. Therefore, improved rate capability of MCG over MC could be attributed to the improved electrical conductivity from graphene and facile ion transport within the 2D ordered mesoporous carbon.

Electrochemical impedance spectroscopy measurements further confirm the favorable performance of MCG, especially ionic conduction pathways. This can be deduced from an analysis of the frequency response of the capacitance. Fig. 6e indicates an analysis of the frequency response of its capacitance (C_{real} and $C_{imaginary}$). The relaxation time constant, τ_0, is a factor of merit, can be calculated as $\tau_0 = 1/f_0$, where f_0 is the characteristic frequency of the system obtained for a phase angle of 45°, and corresponding to the maximum on the dispersed energy curve.[83] The ion transport behaviour is quantitatively evaluated using the relaxation time constant (τ_0).[27, 83, 84] The τ_0 of MCG was calculated to be 1.26 s (0.8 Hz), which is much smaller than that of MC (31.6 s). The time constant reflects the relaxation time of inner-pore ion transport, and the smaller the time constant the easier the ion transport. These results clearly provide evidence of the advantages of the presence of ionic conduction pathways in the electroactive material. Furthermore, τ_0 of MCG is considerably smaller than those measured for commercial activated carbon Supra (8.5 s), advanced activated carbons (10 s) and carbide-derived carbons (6.7 s) in an organic electrolyte.[13, 75, 85] Additionally, the specific capacitance values calculated from CV, galvanostatic curves, and EIS should be in agreement. the specific capacitance values are C_{CV} = 255 F g^{-1}, $C_{galvanostatic}$ = 276 F g^{-1}, and C_{EIS} = 266 F g^{-1}, from CV, galvanostatic, and EIS experiments, respectively. These values were normalized with respect to the mass of a single electrode, and we believe that they are in strong agreement. To investigate the cycling stability of MCG, it was subjected to long-term galvanostatic charge/discharge cycling at a current density of 30 A g^{-1} (Fig. 6f). After 8000 cycles, the system still retained 97% of its initial capacitance, indicating the excellent cycling stability of MCG, which is significant for its practical applications.

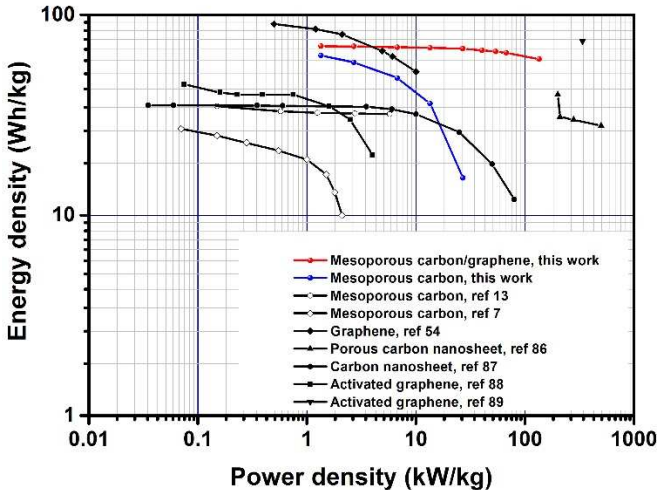

Fig. 7. Comparison of Ragone plots of the MCG-cell prepared in this study with those of previously reported mesoporous carbons and graphene

The Ragone plots displayed in Fig. 7 clearly demonstrate the ultrahigh-power performance of the MCG-based two-electrode symmetric EDLC cell (denoted as MCG-cell). The superior performance of MCG-cell was highlighted by its ability to deliver more power compared to the MC-based two-electrode symmetric EDLC cell (denoted as MC-cell). At a power density of 1.4 kW kg^{-1}, MCG-cell and MC-cell show similar energy densities of 69.8 and 62.6 Wh kg^{-1}, respectively. However, MCG-cell maintain the energy density of 67.7 Wh kg^{-1} as the power density increased to 27 kW kg^{-1}, while MC-cell shows a large drop in the energy density to 15.3 Wh kg^{-1}. Furthermore, MCG-cell maintains the energy density of 60.2 Wh kg^{-1} as the power density increased to 135 kW kg^{-1}. Such a significant energy density drop of MC-cell is caused by its large ESR due to the large ion diffusion resistance and low electrical conductivity with slow time response. Furthermore, MCG showed superior performance compared to mesoporous carbons and graphene in an organic electrolyte or an ionic liquid, as previously reported in the literature.[7, 13, 54, 86-89]

Conclusions

In summary, a two dimentional highly ordered mesoporous carbon/graphene nanocomposite was successfully synthesized by the replication of KIT-6/graphene nanocomposite. The synthesized MCG with high surface area (1179 m^2 g^{-1}) showed the superbspecific capacitance value of 276 F g^{-1} at 1 A g^{-1} and maintains 86% of initial capacitance even at extremely high discharge current of 100 A g^{-1} in 1.0 M $TEABF_4$/AN. Most importantly, MCG based two-electrode symmetric EDLC cell shows a very high power density of 135 kW kg^{-1} at energy

Journal of Materials Chemistry A Accepted Manuscript

This journal is © The Royal Society of Chemistry [year]

density of 60 Wh kg^{-1}. The outstanding performance should be ascribed to the high electronic and ionic conductivity of MCG due to the introduction of graphene and unique 2D morphology. It was demonstrated that the MCG could be used as a kind of promising electrode materials for high-performance EDLCs.

Acknowledgement

This work was supported by the Energy, Efficiency and Resources of the Korea Institute of Energy Technology Evaluation and Planning (KETEP) grant funded by the Ministry of Knowledge Economy, Korean government (No: 20122010100140).

Notes and references

[a] *Department of Materials Science & Engineering, Yonsei University, 50 Yonsei-ro, Seodaemun-gu, Seoul 120-749, Republic of Korea. Fax: +82-2-312-5375; Tel: +82-2-365-7745; E-mail: kbkim@yonsei.ac.kr*

[b] *Energy Efficient Materials Team, Energy & Environmental Division, Korea Institute of Ceramic Engineering & Technology, 233-5 Gasan-dong, Guemcheon-gu, Seoul 153-801, Republic of Korea. Fax: +82-2-3282-2475; Tel: +82-2-3282-2463; E-mail: rkc@kicet.re.kr*

† Electronic Supplementary Information (ESI) available: [TEM images of KIR-6/graphene and mesoporous carbon/graphene; TEM images of mesoporous carbon; SEM image of mesoporous carbon/graphene; C1s XPS spectra of mesoporous carbon/graphene and mesoporous carbon; high rate capability of mesoporous carbon/graphene and mesoporous carbon]. See DOI: 10.1039/b000000x/

1. M. Winter and R. J. Brodd, *Chemical Reviews*, 2004, 104, 4245-4270.
2. J. R. Miller and P. Simon, *Science*, 2008, 321, 651-652.
3. B. E. Conway, *Electrochemical Supercapacitors. Scientific Fundamentals and Technological Applications*, Kluwer Academic Publishers, Plenum Press: New York, 1999.
4. B. G. Choi, M. Yang, W. H. Hong, J. W. Choi and Y. S. Huh, *Acs Nano*, 2012, 6, 4020-4028.
5. M. J. Bleda-Martínez, J. A. Maciá-Agulló, D. Lozano-Castelló, E. Morallón, D. Cazorla-Amorós and A. Linares-Solano, *Carbon*, 2005, 43, 2677-2684.
6. M. A. Lillo-Ródenas, D. Cazorla-Amorós and A. Linares-Solano, *Carbon*, 2003, 41, 267-275.
7. C. Liu, Z. Yu, D. Neff, A. Zhamu and B. Z. Jang, *Nano Lett*, 2010, 10, 4863-4868.
8. L. Sun, C. Tian, M. Li, X. Meng, L. Wang, R. Wang, J. Yin and H. Fu, *Journal of Materials Chemistry A*, 2013, 1, 6462-6470.
9. G. Wang, L. Zhang and J. Zhang, *Chemical Society Reviews*, 2012, 41, 797-828.
10. C. Liu, F. Li, L.-P. Ma and H.-M. Cheng, *Advanced materials*, 2010, 22, E28-E62.
11. S. Yoon, J. Lee, T. Hyeon and S. M. Oh, *Journal of The Electrochemical Society*, 2000, 147, 2507-2512.
12. P. Simon and Y. Gogotsi, *Nat Mater*, 2008, 7, 845-854.
13. Y. Korenblit, M. Rose, E. Kockrick, L. Borchardt, A. Kvit, S. Kaskel and G. Yushin, *Acs Nano*, 2010, 4, 1337-1344.
14. L. Zhang and G. Shi, *The Journal of Physical Chemistry C*, 2011, 115, 17206-17212.
15. L. L. Zhang and X. S. Zhao, *Chem Soc Rev*, 2009, 38, 2520-2531.
16. E. Frackowiak and F. Beguin, *Carbon*, 2001, 39, 937-950.
17. Z. Lei, N. Christov and X. S. Zhao, *Energy & Environmental Science*, 2011, 4, 1866-1873.
18. D.-W. Wang, F. Li, M. Liu, G. Q. Lu and H.-M. Cheng, *Angewandte Chemie*, 2008, 120, 379-382.
19. L. Wang, L. Sun, C. Tian, T. Tan, G. Mu, H. Zhang and H. Fu, *RSC Advances*, 2012, 2, 8359-8367.
20. M. Li, J. Ding and J. M. Xue, *Journal of Materials Chemistry A*, 2013, 1, 7469-7476.
21. K. Sheng, Y. Sun, C. Li, W. Yuan and G. Shi, *Scientific reports*, 2012, 2, 247.
22. Z. Bo, Z. Wen, H. Kim, G. Lu, K. Yu and J. Chen, *Carbon*, 2012, 50, 4379-4387.
23. C. Vix-Guterl, S. Saadallah, K. Jurewicz, E. Frackowiak, M. Reda, J. Parmentier, J. Patarin and F. Beguin, *Materials Science and Engineering: B*, 2004, 108, 148-155.
24. K. Jurewicz, C. Vix-Guterl, E. Frackowiak, S. Saadallah, M. Reda, J. Parmentier, J. Patarin and F. Béguin, *Journal of Physics and Chemistry of Solids*, 2004, 65, 287-293.
25. W. Xing, S. Z. Qiao, R. G. Ding, F. Li, G. Q. Lu, Z. F. Yan and H. M. Cheng, *Carbon*, 2006, 44, 216-224.
26. H.-Q. Li, J.-Y. Luo, X.-F. Zhou, C.-Z. Yu and Y.-Y. Xia, *Journal of The Electrochemical Society*, 2007, 154, A731-A736.
27. D.-W. Wang, F. Li, M. Liu, G. Q. Lu and H.-M. Cheng, *The Journal of Physical Chemistry C*, 2008, 112, 9950-9955.
28. Y.-S. Lin and C. L. Haynes, *Journal of the American Chemical Society*, 2010, 132, 4834-4842.
29. C. Portet, G. Yushin and Y. Gogotsi, *Journal of The Electrochemical Society*, 2008, 155, A531-A536.
30. T. W. Kim, R. Ryoo, K. P. Gierszal, M. Jaroniec, L. A. Solovyov, Y. Sakamoto and O. Terasaki, *Journal of Materials Chemistry*, 2005, 15, 1560-1571.
31. T. W. Kim, I. S. Park and R. Ryoo, *Angew Chem Int Edit*, 2003, 42, 4375-4379.
32. M. Kruk, M. Jaroniec, R. Ryoo and S. H. Joo, *J Phys Chem B*, 2000, 104, 7960-7968.
33. C. H. Kim, D. K. Lee and T. J. Pinnavaia, *Langmuir*, 2004, 20, 5157-5159.
34. Y. D. Xia and R. Mokaya, *Advanced materials*, 2004, 16, 1553-+.
35. F. B. Su, J. H. Zeng, X. Y. Bao, Y. S. Yu, J. Y. Lee and X. S. Zhao, *Chemistry of Materials*, 2005, 17, 3960-3967.
36. R. M. Grudzien, B. E. Grabicka and M. Jaroniec, *Appl Surf Sci*, 2007, 253, 5660-5665.
37. Z. W. Dong, F. Ye and H. J. Zhang, *Mater Lett*, 2009, 63, 2343-2345.
38. A. B. Fuertes and S. Alvarez, *Carbon*, 2004, 42, 3049-3055.
39. S. Yang, X. Feng, L. Wang, K. Tang, J. Maier and K. Mullen, *Angewandte Chemie*, 2010, 49, 4795-4799.
40. A. K. Geim and K. S. Novoselov, *Nat Mater*, 2007, 6, 183-191.
41. D. R. Dreyer, S. Park, C. W. Bielawski and R. S. Ruoff, *Chemical Society Reviews*, 2010, 39, 228-240.
42. S. Stankovich, D. A. Dikin, R. D. Piner, K. A. Kohlhaas, A. Kleinhammes, Y. Jia, Y. Wu, S. T. Nguyen and R. S. Ruoff, *Carbon*, 2007, 45, 1558-1565.
43. D. Yang, A. Velamakanni, G. Bozoklu, S. Park, M. Stoller, R. D. Piner, S. Stankovich, I. Jung, D. A. Field, C. A. Ventrice and R. S. Ruoff, *Carbon*, 2009, 47, 145-152.
44. S. M. Bak, K. W. Nam, C. W. Lee, K. H. Kim, H. C. Jung, X. Q. Yang and K. B. Kim, *Journal of Materials Chemistry*, 2011, 21, 17309-17315.
45. H.-K. Kim, S.-M. Bak and K.-B. Kim, *Electrochemistry Communications*, 2010, 12, 1768-1771.
46. G.-P. Hao, A.-H. Lu, W. Dong, Z.-Y. Jin, X.-Q. Zhang, J.-T. Zhang and W.-C. Li, *Advanced Energy Materials*, 2013, 3, 1421-1427.
47. J. Yan, T. Wei, B. Shao, Z. Fan, W. Qian, M. Zhang and F. Wei, *Carbon*, 2010, 48, 487-493.
48. D.-W. Wang, F. Li, J. Zhao, W. Ren, Z.-G. Chen, J. Tan, Z.-S. Wu, I. Gentle, G. Q. Lu and H.-M. Cheng, *Acs Nano*, 2009, 3, 1745-1752.
49. L.-L. Shao, M. Chen, T.-Z. Ren and Z.-Y. Yuan, *Journal of Power Sources*, 2015, 274, 791-798.
50. S. Sigalov, M. D. Levi, G. Salitra, D. Aurbach, A. Jänes, E. Lust and I. C. Halalay, *Carbon*, 2012, 50, 3957-3960.
51. D. Zhang, X. Wen, L. Shi, T. Yan and J. Zhang, *Nanoscale*, 2012, 4, 5440-5446.

Journal of Materials Chemistry A Accepted Manuscript

52. C.-W. Lee, K. C. Roh and K.-B. Kim, *Nanoscale*, 2013, 5, 9604-9608.
53. S. Park, J. An, J. R. Potts, A. Velamakanni, S. Murali and R. S. Ruoff, *Carbon*, 2011, 49, 3019-3023.
54. M. Sevilla and A. B. Fuertes, *Acs Nano*, 2014, 8, 5069-5078.
55. J. Yan, Q. Wang, T. Wei, L. Jiang, M. Zhang, X. Jing and Z. Fan, *Acs Nano*, 2014, DOI: 10.1021/nn500497k.
56. M. D. Stoller and R. S. Ruoff, *Energy & Environmental Science*, 2010, 3, 1294-1301.
57. D. Puthusseri, V. Aravindan, S. Madhavi and S. Ogale, *Energy & Environmental Science*, 2014, 7, 728-735.
58. S.-H. Park, S.-M. Bak, K.-H. Kim, J.-P. Jegal, S.-I. Lee, J. Lee and K.-B. Kim, *Journal of Materials Chemistry*, 2011, 21, 680-686.
59. C. Weidenthaler, *Nanoscale*, 2011, 3, 792-810.
60. K. S. W. Sing, D. H. Everett, R. A. W. Haul, L. Moscou, R. A. Pierotti, J. Rouquerol and T. Siemieniewska, *Pure and Applied Chemistry*, 1985, 57, 603-619.
61. K. P. Gierszal, T. W. Kim, R. Ryoo and M. Jaroniec, *J Phys Chem B*, 2005, 109, 23263-23268.
62. W. Dai, M. Zheng, Y. Zhao, S. Liao, G. Ji and J. Cao, *Nanoscale Res Lett*, 2009, 5, 103-107.
63. J.-y. Luo, Y.-g. Wang, H.-m. Xiong and Y.-y. Xia, *Chemistry of Materials*, 2007, 19, 4791-4795.
64. D. D. Asouhidou, K. S. Triantafyllidis, N. K. Lazaridis, K. A. Matis, S. S. Kim and T. J. Pinnavaia, *Microporous and Mesoporous Materials*, 2009, 117, 257-267.
65. H. Yang, Yan, Y. Liu, F. Zhang, R. Zhang, Y. YanMeng, M. Li, S. Xie, B. Tu and D. Zhao, *The Journal of Physical Chemistry B*, 2004, 108, 17320-17328.
66. D. Yang, A. Velamakanni, G. Bozoklu, S. Park, M. Stoller, R. D. Piner, S. Stankovich, I. Jung, D. A. Field, C. A. Ventrice Jr and R. S. Ruoff, *Carbon*, 2009, 47, 145-152.
67. T. C. Chiang and F. Seitz, *Annalen der Physik*, 2001, 10, 61-74.
68. S. Yumitori, *Journal of Materials Science*, 2000, 35, 139-146.
69. Y. Zhu, S. Murali, W. Cai, X. Li, J. W. Suk, J. R. Potts and R. S. Ruoff, *Advanced materials*, 2010, 22, 3906-3924.
70. C. Nethravathi and M. Rajamathi, *Carbon*, 2008, 46, 1994-1998.
71. A. V. Murugan, T. Muraliganth and A. Manthiram, *Chemistry of Materials*, 2009, 21, 5004-5006.
72. H.-L. Guo, X.-F. Wang, Q.-Y. Qian, F.-B. Wang and X.-H. Xia, *Acs Nano*, 2009, 3, 2653-2659.
73. L. Wang, S. Lin, K. Lin, C. Yin, D. Liang, Y. Di, P. Fan, D. Jiang and F.-S. Xiao, *Microporous and Mesoporous Materials*, 2005, 85, 136-142.
74. H. Yang, Q. Shi, X. Liu, S. Xie, D. Jiang, F. Zhang, C. Yu, B. Tu and D. Zhao, *Chemical Communications*, 2002, DOI: 10.1039/B209233F, 2842-2843.
75. L. Wei, M. Sevilla, A. B. Fuertes, R. Mokaya and G. Yushin, *Advanced Energy Materials*, 2011, 1, 356-361.
76. W.-w. Liu, X.-b. Yan, J.-w. Lang, J.-b. Pu and Q.-j. Xue, *New Journal of Chemistry*, 2013, 37, 2186-2195.
77. Y. Li, Z. Li and P. K. Shen, *Advanced materials*, 2013, 25, 2474-2480.
78. L. Hou, L. Lian, D. Li, G. Pang, J. Li, X. Zhang, S. Xiong and C. Yuan, *Carbon*, 2013, 64, 141-149.
79. H. Xu, Q. Gao, H. Guo and H. Wang, *Microporous and Mesoporous Materials*, 2010, 133, 106-114.
80. G. Lota, T. A. Centeno, E. Frackowiak and F. Stoeckli, *Electrochimica Acta*, 2008, 53, 2210-2216.
81. X. Li, C. Han, X. Chen and C. Shi, *Microporous and Mesoporous Materials*, 2010, 131, 303-309.
82. Y. S. Yun, S. Y. Cho, J. Shim, B. H. Kim, S.-J. Chang, S. J. Baek, Y. S. Huh, Y. Tak, Y. W. Park, S. Park and H.-J. Jin, *Advanced materials*, 2013, 25, 1993-1998.
83. C. Portet, G. Yushin and Y. Gogotsi, *Carbon*, 2007, 45, 2511-2518.
84. T. Thomberg, A. Jänes and E. Lust, *Journal of Electroanalytical Chemistry*, 2009, 630, 55-62.
85. P. L. Taberna, P. Simon and J. F. Fauvarque, *Journal of The Electrochemical Society*, 2003, 150, A292.
86. X. He, P. Ling, J. Qiu, M. Yu, X. Zhang, C. Yu and M. Zheng, *Journal of Power Sources*, 2013, 240, 109-113.
87. W. Qian, F. Sun, Y. Xu, L. Qiu, C. Liu, S. Wang and F. Yan, *Energy & Environmental Science*, 2014, 7, 379-386.
88. L. L. Zhang, X. Zhao, M. D. Stoller, Y. Zhu, H. Ji, S. Murali, Y. Wu, S. Perales, B. Clevenger and R. S. Ruoff, *Nano Letters*, 2012, 12, 1806-1812.
89. T. Kim, G. Jung, S. Yoo, K. S. Suh and R. S. Ruoff, *Acs Nano*, 2013, 7, 6899-6905.

Journal of Materials Chemistry A Accepted Manuscript

This journal is © The Royal Society of Chemistry [year]

A Two Dimensional Highly Ordered Mesoporous Carbon/Graphene Nanocomposite for Supercapacitors: Effect of Electrical and Ionic Conduction Pathways

Chang-Wook Lee,[a] Seung-Beom Yoon,[a] Hyun-Kyung Kim,[b] Joah Han,[b] Kwang Chul Roh,*[b] and Kwang-Bum Kim*[a]

Table of contents entry

A highly ordered mesoporous carbon/graphene nanocomposite was synthesized by replicating a KIT-6/graphene nanocomposite. The MCG exhibited a high surface area of 1179 $m^2 g^{-1}$ and a large total pore volume of 0.94 $cm^3 g^{-1}$ with a bimodal pore system. By taking advantage of its large surface area and high electrical conductivity, the result from electrochemical characterization of the MCG as the electrode materials in supercapacitor shows a very high power density of 135 kW kg^{-1} with energy density of 60 Wh kg^{-1}.

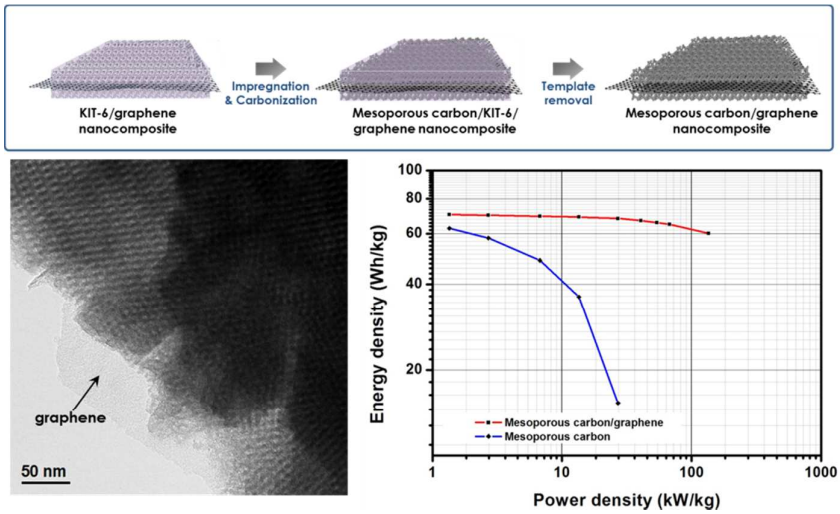

Journal of Materials Chemistry A Accepted Manuscript